BIOCHEMISTRY

 Volume 45, Number 44 November 7, 2006

Articles

Understanding the Folding Mechanism of an α-Helical Hairpin†

Deguo Du and Feng Gai*

Department of Chemistry, University of Pennsylvania, Philadelphia, Pennsylvania 19104

Received August 3, 2006; Revised Manuscript Received September 6, 2006

ABSTRACT: The α-helical hairpin is the fundamental building block of the widespread helix−turn−helix DNA binding motif. With two antiparallel helices connected by a reverse turn, the α-helical hairpin structure may be regarded as a "supersecondary structural element" and, therefore, could exhibit rather unique folding properties. So far, the folding mechanism of α-helical hairpins has not been studied in detail and remains elusive. Herein, we examine the effects of the turn, the hydrophobic cluster, and a disulfide cross-linker on the folding kinetics of a designed α-helical hairpin, Z34C, using an infrared temperature-jump (*T*-jump) method in conjunction with site-specific mutagenesis. Our results show that Z34C folds with an ultrafast rate (~4.0×10^5 s^{-1}) and support a folding mechanism in which the rate-limiting step corresponds to the formation of the reverse turn. On the other hand, the hydrophobic cluster and the disulfide cross-linker appear to largely stabilize the native state but not the folding transition state.

The α-helical hairpin (or helix−turn−helix motif) is a common structural motif and has been shown to be a critical element of DNA-binding proteins (*1*). Similar to that of a *β*-hairpin, the structure of an α-helical hairpin consists of two antiparallel helices connected by a reverse turn. Despite the α-helical hairpin being a widespread motif (*2*) and responsible for a diversity of functions, its folding mechanism has not been systematically studied and thus remains elusive. Furthermore, it has been suggested that the α-helical hairpin structure may resemble a protein folding intermediate (*3*); hence, its folding could be used to test the existing protein folding models (*4*−*6*). Herein, we have studied the folding kinetics of a designed α-helical hairpin (*7*) with the aim of elucidating the sequence of key kinetic events along the folding pathway of the helix−turn−helix supersecondary structural motif.

While most α-helical hairpins in isolation are incapable of folding, Braisted and Wells (*8*) have recently shown that a 38-residue peptide, Z38, which is a truncated form of the 59-residue B-domain of protein A and was selected by phage display, folds into a helical hairpin conformation in aqueous solution. While Z38 is only marginally stable, Starovasnik et al. (*7*) showed that a disulfide-bonded variant of Z38, i.e., Z34C, exhibits dramatically enhanced stability. Their circular dichroism (CD)[1] experiments indicated that Z34C unfolds cooperatively with an increase in temperature and the middle point of the transition occurs at ~53 °C. In addition, they showed that Z34C is highly soluble and remains monomeric in aqueous solution, and its NMR structure is composed of two α-helices (Figure 1), in which a four-residue reverse turn (DPNL) connects helix 1 (M8−L18) with helix 2 (E25−C39).

Moreover, the results of Starovasnik et al. indicated that the disulfide cross-linker in Z34C, formed between Cys10

† Supported by the National Science Foundation (CHE-0094077 and DMR05−20020).

* To whom correspondence should be addressed. Telephone: (215) 573-6256. Fax: (215) 573-2112. E-mail: gai@sas.upenn.edu.

[1] Abbreviations: CD, circular dichroism; FTIR, Fourier transform infrared; *T*-jump, temperature jump; HTH, helix−turn−helix.

10.1021/bi0615745 CCC: $33.50
Published on Web 10/17/2006

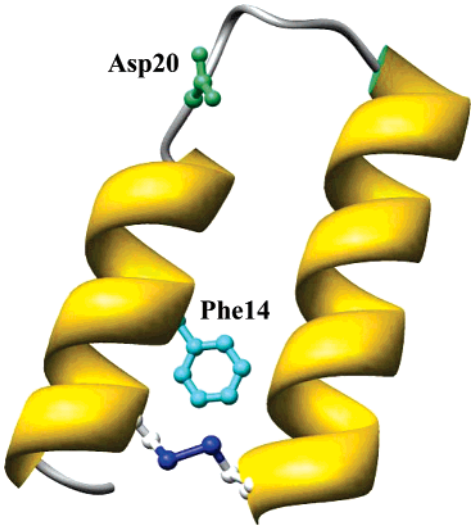

FIGURE 1: NMR structure of Z34C (PDB entry d34c). The disulfide bond formed between Cys10 and Cys39 is colored blue. Also shown are side chains of Phe14 and Asp20. The sequence of Z34C is ^{6}FNMQCQRRFY-^{16}EALHDPNLNE-^{26}EQRNAKIKSI-^{36}RDDC.

and Cys39, does not appear to distort the intrinsic structure of Z38 but rather to stabilize its α-helical hairpin fold (*7*). Therefore, Z34C constitutes a good model system for understanding, from a kinetic point of view, why the disulfide cross-linker stabilizes the helix−turn−helix structure. One possibility is that it increases the folding rate by acting as a nucleation site, whereas an alternative one is that it stabilizes the folded conformation by merely acting as a conformational constraint, which effectively increases the unfolding free energy barrier and consequently decreases the unfolding rate. In a similar manner, the underlying effect of other structural elements, such as the reverse turn and the hydrophobic cluster, on the stability of the α-helical hairpin may also be revealed by studying how they affect the folding−unfolding free energy barrier through mutation. To reveal the kinetic role of some of the key structural elements in the α-helical hairpin motif, we herein study the folding kinetics of the wild type and five mutants of Z34C. The first group of mutants (D20A, P21G, and P21N/N22P) was chosen because these mutations affect the stability of the reverse turn, whereas the second group of mutants (F14A and F14A/I35A) was chosen because both Phe14 and Ile35 have been shown to be an integral part of the hydrophobic cluster of Z34C (*7*). Additionally, the kinetic role of the disulfide cross-linker was investigated by studying the folding kinetics of the un-cross-linked counterparts of Z34C, D20A, and F14A. Taken together, these studies allowed us not only to reveal the underlying mechanism of stabilization of these key structural elements, which have ramifications on protein design (*3*, *7*, *9*, *10*), but also to generate a comprehensive description of the folding mechanism of Z34C. Our results support an α-helical hairpin folding mechanism in which the rate-limiting step corresponds to the formation of the reverse turn, whereas the hydrophobic cluster is formed at the downhill side of the folding free energy barrier, similar to the proposed kinetic folding mechanism of β-hairpins (*11*, *12*).

The folding kinetics of these peptides were studied by a laser-induced temperature-jump infrared method (*13*, *14*), while the mutational studies provide information for understanding the folding transition state (*15*). The *T*-jump technique has been reviewed previously (*16*). Briefly, it provides a means of quickly perturbing the temperature of a system and, consequently, producing a nonequilibrium state. The relaxation kinetics of the perturbed system toward a new equilibrium position, which were probed in this case by monitoring the amide I′ absorbance of the α-helical hairpin, provide information for both the folding and unfolding kinetics. The amide I′ band of polypeptides is due mainly to the amide C═O stretch vibration and is an established global conformational reporter of secondary structures because of its sensitivity to structural determinants (*16*−*22*).

MATERIALS AND METHODS

Peptides were synthesized using the standard fluoren-9-ylmethoxycarbonyl (Fmoc)-based solid-phase method on a PS3 peptide synthesizer (Protein Technologies), purified by reverse-phase chromatography, and verified by matrix-assisted laser desorption ionization mass spectroscopy. The residual trifluoroacetic acid from peptide synthesis, which has an IR band overlapping with the amide I′ band of polypeptides, was removed by multiple lyophilizations against a 0.1 M DCl solution. The disulfide-bonded or oxidized sample (i.e., Z34C, D20A, P21A, P21N/N22P, F14A, and F14A/I35A) was prepared by using air bubbles to oxidize the initially purified peptide product at pH 7.5, and the resultant product was further purified by HPLC. The un-cross-linked or reduced sample (i.e., Z34C-R, D20A-R, and F14A-R) was prepared using tris(2-carboxyethyl)-phosphine hydrochloride (TCEP) as the reducing agent. The concentration of the TCEP was kept at least 10 times greater than that of the peptide.

CD thermal melting curves were obtained on an Aviv 62A DS spectropolarimeter (Aviv Associates) with a 1 mm sample holder. The peptide concentration was ∼50 μM in a 20 mM phosphate D_2O buffer solution (pH* 7), determined optically using the tyrosine absorbance at 276 nm using an ϵ_{276} of 1450 cm^{-1} M^{-1}.

Temperature-dependent Fourier transform infrared (FTIR) spectra were collected on a Magna-IR 860 spectrometer (Nicolet) using 2 cm^{-1} resolution. A CaF_2 sample cell that was divided into two compartments with a Teflon spacer was used to allow the separate measurements of the sample and the reference under identical conditions. The optical path length of the sample cell was determined to be 52 μm by its interference fringes obtained from the transmittance signal of the empty cell. Temperature control with ±0.2 °C precision was obtained with a thermostated copper block. To correct slow instrument drifts, both the sample and reference sides of the sample cell were moved in and out of the IR beam alternately, and each time a spectrum corresponding to an average of eight scans was collected. The final result was usually an average of 32 such spectra, both for the sample and for the reference. For both static and time-resolved IR measurements, the sample was prepared by directly dissolving lyophilized solids in 20 mM phosphate D_2O buffer (pH* 7), and the final concentration was 1−2 mM.

The *T*-jump IR setup has been described in detail elsewhere (*13*, *14*). Briefly, a heating pulse at ∼1.9 μm (3 ns and 10 mJ) was used to generate a *T*-jump of ∼10 °C. Transient absorbance changes induced by this *T*-jump pulse were probed by a continuous wave IR diode laser and a 50

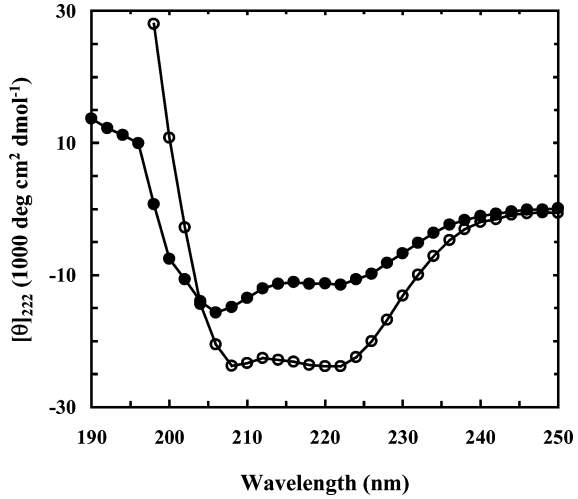

FIGURE 2: CD spectra of Z34C (○) and its un-cross-linked counterpart, Z34C-R (●).

MHz HgCdTe detector. As in the static FTIR measurement, a sample cell with dual compartments was used to allow the separate measurements of the absorbance changes of the sample and reference under identical conditions. Measurements with the reference (buffer) provide the information needed for both *T*-jump amplitude calibration and background subtraction.

RESULTS

Equilibrium CD Study. As shown (Figure 2), the far-UV CD spectra of Z34C and its un-cross-linked counterpart (i.e., Z34C-R) at 4 °C exhibit typical characteristics of helical proteins, with two minima at 208 and 222 nm. However, the mean residue ellipticity of Z34C-R at 222 nm is only ~40% of that of Z34C, indicating that the un-cross-linked peptide is much less stable than cross-linked Z34C. Therefore, these results confirm the stabilizing role of the disulfide cross-linker (*7*). Moreover, the CD spectra of the mutants (data not shown) show that while the helicities of D20A, P21A, and F14A are almost identical to that of the parent at 4 °C, both P21N/N22P and F14A/I35A exhibit a much lower overall helical content, thereby indicating that a suitable turn sequence and a strong interstrand hydrophobic cluster are critically important for maintaining the α-helical hairpin conformation. Further thermal unfolding studies, which were carried out by monitoring the ellipticities of these peptides at 222 nm as a function of temperature (Figure 3), allowed us to quantitatively determine how these mutations affect the native stability of Z34C.

Specifically, we have globally fit the thermal CD denaturation curves of Z34C and its mutants to the following two-state model (Figure 3)

$$\theta(T) = \frac{\theta_F(T) + K_{eq}(T) \times \theta_U(T)}{1 + K_{eq}(T)} \quad (1)$$

$$K_{eq}(T) = \exp[-\Delta G(T)/RT] \quad (2)$$

$$\Delta G(T) = \Delta H_m + \Delta C_p(T - T_m) - T[\Delta S_m + \Delta C_p \ln(T/T_m)] \quad (3)$$

where $\theta_F(T)$ is the folding CD baseline, $\theta_U(T)$ is the unfolding CD baseline, $K_{eq}(T)$ is the equilibrium constant for unfolding, T_m ($=\Delta H_m/\Delta S_m$) is the thermal melting temperature, ΔH_m and ΔS_m are the enthalpy and entropy changes at T_m, respectively, and ΔC_p is the heat capacity change associated with unfolding, which has been assumed here to be temperature-independent. In the global fit, both $\theta_F(T)$ and $\theta_U(T)$ were treated as linear functions of temperature; i.e., $\theta_F(T) = a_i + bT$, and $\theta_U(T) = c_i + dT$, where b and d were assumed to be the same for all of the peptides and were treated as global parameters whereas a_i and c_i were treated as local parameters. Because of the lack of a folded CD baseline, the folding thermodynamics of the un-cross-linked peptides, i.e., Z34C-R, D20A-R, and F14A-R, as well as P21N/N22P and F14A/I35A cannot be rigorously determined. However, by assuming that their folded CD baseline is the same as that of Z34C, we were able to estimate their thermal stabilities. The corresponding thermodynamic parameters resulted from the global fit are listed in Table 1. As expected, all of the mutations resulted in a T_m lower than that of Z34C, indicating that both the turn sequence and the hydrophobic interaction are important determinants of the α-helical hairpin stability. In particular, when the middle two residues in the DPNL turn swapped positions, the native stability was severely reduced.

Equilibrium FTIR Study. The thermal unfolding transition of these peptides was further investigated by examining their amide I′ bands. The amide I′ band of polypeptides arises mainly from the stretching vibration of the backbone carbonyls. Because of its sensitivity to structural parameters, the amide I′ band is an established indicator of protein secondary structures (*17*). For example, helical amides, depending on their solvation status, can exhibit an amide I′ band centered at either ~1630 or 1644 cm^{-1} (*20*, *21*). As shown (Figure 4), the difference FTIR spectra of Z34C, which were generated by subtracting the FTIR spectrum collected at 8.2 °C from those collected at higher temperatures, show a negative-going feature at ~1632 cm^{-1} and a shoulder at ~1644 cm^{-1}, due to the increasingly decreased helical hairpin population at higher temperatures. Concomitantly, a positive-going signal at ~1670 cm^{-1} increases with temperature, because of the increase in the population of the unfolded and nonhelical conformations. Previously, we have shown that the optical density (OD) change at ~1670 cm^{-1} is the best IR indicator for monitoring the thermal unfolding transition of helical proteins (*20*). Indeed, the thermal denaturation measured by the increase in the OD at 1670 cm^{-1} for Z34C closely matches that reported by CD (inset of Figure 4), indicating that both methods report the same unfolding process. Other peptides exhibit similar behaviors.

Infrared T-Jump Study. The *T*-jump-induced relaxation kinetics of these peptides were monitored by time-resolved IR spectroscopy (*13*, *14*). As shown (Figure 5), the *T*-jump-induced relaxations exhibited two distinct phases. The fast phase was limited by instrumentation and, according to our early interpretation, was assigned to temperature-induced spectral changes, such as shift and broadening, although imperfect background subtraction would also contribute to this phase, whereas the slow phase could be modeled by first-order kinetics. For a fixed *T*-jump amplitude, the magnitude of the slow phase first increases and then decreases with the

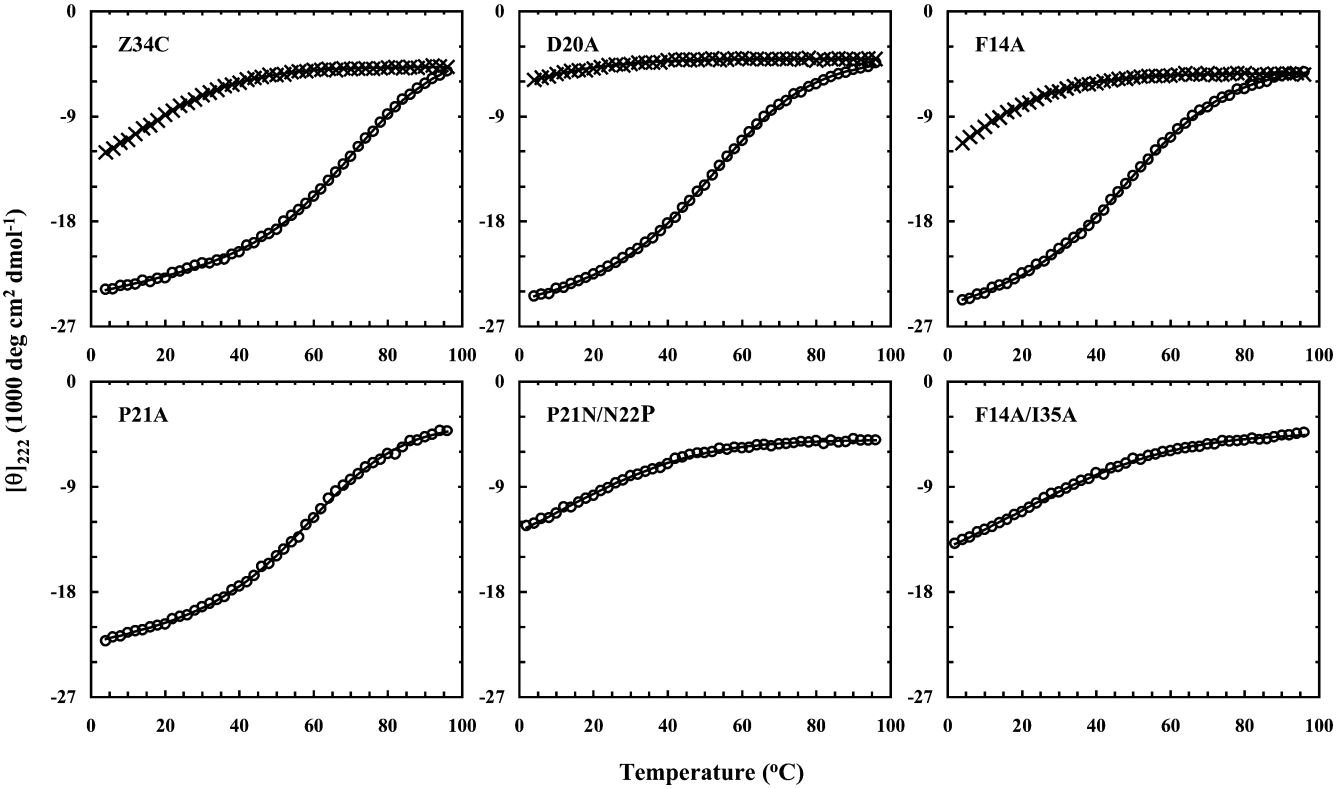

FIGURE 3: Thermal unfolding CD curves of Z34C and its mutants (empty circles represent data for the cross-linked form and crosses data for the un-cross-linked form), as indicated. Lines are fits to the two-state model described in the text.

Table 1: Unfolding Thermodynamic Parameters Obtained from Equilibrium CD Measurements[a]

peptide	ΔH_m (kcal/mol)	ΔS_m (cal K^{-1} mol^{-1})	ΔC_p (cal K^{-1} mol^{-1})	T_m (°C)
Z34C	18.8 ± 1.3	54.6 ± 4.9	168 ± 45	71.6 ± 1.5
Z34C-R	*3.0*	*11.4*	*197*	*−13.2*
D20A	16.2 ± 0.7	49.4 ± 3.8	118 ± 34	54.6 ± 0.9
D20A-R	−	−	−	−
P21A	17.5 ± 1.5	52.2 ± 6.1	121 ± 50	61.1 ± 1.2
P21N/N22P	*0.1*	*0.4*	*152*	*−25.2*
F14A	15.0 ± 0.9	46.3 ± 4.2	85 ± 30	51.3 ± 1.1
F14A-R	*5.9*	*22.8*	*131*	*−15.2*
F14A/I35A	*3.3*	*12.2*	*115*	*0.5*

[a] Italic numbers were estimated (see the text).

increase in the final temperature, indicating that this component probes the cooperative thermal folding−unfolding transition reported by the static CD and IR measurements. Therefore, the observed relaxation rate constants (k_{obs}) of these peptides, except D20A-R, were further separated into folding (k_f) and unfolding (k_u) rate constants (Figure 6) based on the following relationships for two-state folding: $k_{obs} = k_f + k_u$ and $K_{eq} = k_u/k_f$, where K_{eq} is the equilibrium constant for unfolding and was calculated using the thermodynamic parameters in Table 1. It is evident that the folding rates of these peptides are very fast and exhibit only weak temperature dependence (Figure 6). Fitting these data to the Eyring equation indeed yielded a relatively small $\Delta H^{\ddagger}$ for folding. For example, the enthalpy of activation for Z34C was determined to be ~0.7 kcal/mol at T_m (note that the $\Delta S^{\ddagger}$ cannot be determined because the pre-exponential factor is not known). Similarly (perhaps also consistently), it has been shown that the folding of β-hairpins also involves a small energetic barrier (*11*, *12*, *22*). Finally, it is worth noting that the rate constants, especially the folding rate constants,

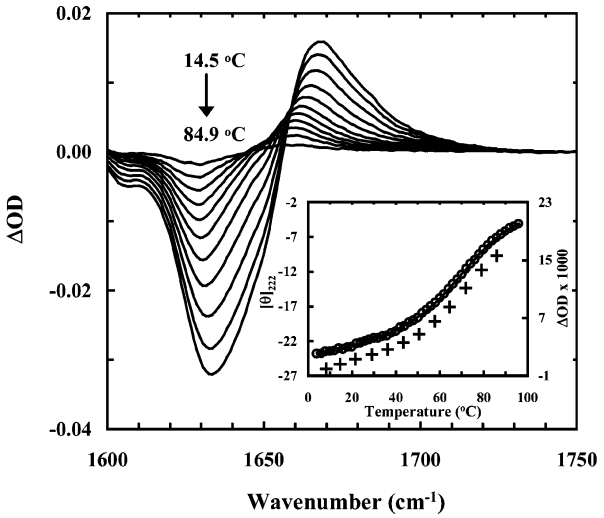

FIGURE 4: Difference FTIR spectra of Z34C. These spectra were generated by subtracting the FTIR spectrum collected at 8.2 °C from those collected at higher temperatures. The inset shows the comparison of the thermal unfoldings of Z34C measured by CD (○) and IR (+), wherein the IR signal corresponds to the ΔOD in the difference spectra at 1670 cm^{-1}.

obtained for those peptides that lack the folded baseline in their thermal unfolding CD curves should be treated as estimates. This is because the unfolding thermodynamics of these peptides (i.e., Z34C-R, F14A-R, P21N/N22P, and F14A/I35A) were estimated using the assumption described above. Since the relaxation rate constants of these peptides were measured in a temperature range within which the unfolded state dominates, the unfolding rate constants determined from the two-state analysis given above are nevertheless more reliable.

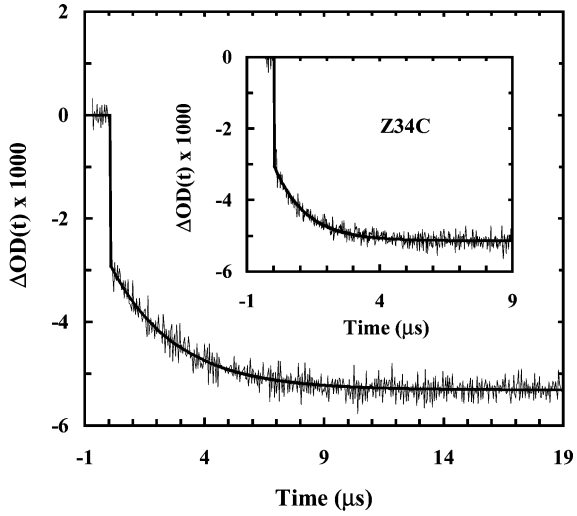

FIGURE 5: Representative relaxation traces of Z34C (inset) and D20A measured with a probing frequency of 1630 cm^{-1}, in response to a *T*-jump of ~10 °C, from 45.1 to 55.1 °C for D20A and from 61.9 to 69.8 °C for Z34C. Smooth lines are fits to the function $\Delta OD(t) = A[1 - B \exp(-t/\tau)]$, where $A = -0.0053$, $B = 0.46$, and $\tau = 2.7$ μs for D20A and $A = -0.0051$, $B = 0.42$, and $\tau = 1.2$ μs for Z34C.

DISCUSSION

The α-helical hairpin is a common structural motif and has been shown to be a critical element of DNA-binding proteins. Moreover, it has been suggested that many "supersecondary structural elements" are derivatives of this so-called helix−turn−helix motif (*2*). Thus, it is probable that the folding of the α-helical hairpin in these supersecondary structures occurs early and acts as a folding nucleus, akin to the proposed role of the β-hairpin in the folding of β-sheet proteins (*23*−*27*). Thus, from a structural evolution point of view, understanding the folding mechanism of the helix−turn−helix motif may help us to better understand the folding mechanism of larger and more complex protein systems (*28*). For this reason, we studied in detail the folding kinetics of an α-helical hairpin peptide designed by Starovasnik et al. (*7*).

Effect of the Disulfide Cross-Linker on the Folding Kinetics. The stability of Z34C is significantly higher compared to that of Z34C-R (Table 1), indicating that the disulfide cross-linker in Z34C plays a crucial role in stabilizing the α-helical hairpin conformation. Kinetically, this can be achieved by either increasing the folding rate, decreasing the unfolding rate, or both. While disulfide linkages are commonly found in proteins (*29*, *30*) and are widely used as a stabilizing strategy in protein design (*31*−*33*), their underlying mechanism responsible for stabilization is not entirely clear (*27*, *34*−*38*). For example, a disulfide cross-linker may simply act as a conformational constraint, which stabilizes the folded state but not the folding transition state. Thus, the increased stability of the native state can be attributed to a slower unfolding rate, because of a (relatively) larger unfolding free energy barrier. On the other hand, a disulfide cross-linker may act as a nucleation site for folding, leading not only to a faster folding rate but also to higher stability. Thus, comparing the folding kinetics of Z34C and Z34C-R would allow us to gain insights into the stabilization mechanism of the disulfide cross-linker.

Within the temperature range in which the data were measured, the folding rate of Z34C depends only weakly on temperature and is ~$(2.5\ \mu s)^{-1}$ at 50 °C (Figure 6 and Table 2), which renders it one of the fastest protein folders known to date (*39*). At first glance, the ultrafast folding behavior of Z34C may be attributed to its disulfide bond because, in principle, such a cross-linker can significantly reduce the entropic cost associated with the search for the native state. To test this hypothesis, we measured the *T*-jump-induced relaxation rate of the un-cross-linked variant of Z34C (i.e., Z34C-R). Interestingly, our results show that while both the folding and unfolding rates of Z34C-R are different from those of Z34C, disruption of the disulfide cross-linker has a much more pronounced effect on the unfolding rate. For example, at 50 °C, the folding rate of Z34C-R is estimated to be ~$(8\ \mu s)^{-1}$, which is only 2.3 times slower than that of its disulfide-bonded counterpart; however, its unfolding rate, ~$(0.3\ \mu s)^{-1}$, is roughly 43 times faster than that of Z34C (Figure 6 and Table 2). While the folding and unfolding rate constants of Z34C-R were obtained on the basis of its folding equilibrium constants estimated from its thermal unfolding CD curve and therefore are subject to a large uncertainty, they nevertheless suggest that the primary role of the disulfide cross-linker in Z34C is to prevent the α-helical hairpin structure from unfolding by decreasing the unfolding rate. Apparently, this is achieved by reducing the conformational flexibility of the molecule, which increases the unfolding but not the folding free energy barrier. Similarly, in the study of the effect of disulfide bonds on the folding kinetics of an all-β-sheet protein, tendamistat, Kiefhaber and co-workers (*27*) also observed that that the main effect of fixed side chain contacts is on the unfolding rate.

In a similar manner, we have also studied the folding thermodynamics and kinetics of the reduced forms of F14A and D20A. Consistent with the results obtained for the wild type, the folding rate of F14A-R was estimated to be ~$(10.4\ \mu s)^{-1}$ at 50 °C, comparable to that of F14A. However, its unfolding rate was estimated to be only ~$(0.2\ \mu s)^{-1}$, significantly faster than that of F14A (Figure 6 and Table 2). Additionally, the unfolding rate of D20A-R was also found to be substantially faster than that of D20A (Figure 6 and Table 2). Therefore, these results further substantiate the above conclusion regarding the kinetic role of the disulfide cross-linker in stabilizing the α-helical hairpin conformation of Z34C. While it has been shown that a disulfide cross-linker could have different effects on the folding thermodynamics and kinetics of large proteins (*37*, *38*, *40*), the results presented here suggest that the major effect of a disulfide bond (and perhaps unstructured cross-linkers) in miniproteins is the prevention of the folding of the two adjacent strands, thereby stabilizing the folded state (*7*, *41*).

Effect of the Turn Sequence on the Folding Kinetics. The reverse turn (DPNL) is another distinct structural element in Z34C. While the apparent role of a turn in proteins is to provide a connection between two secondary structural elements, its sequence composition may have strong effects on the folding thermodynamics and kinetics (*40*, *42*). For example, it is well-established that the turn sequence is one of the key factors that control the stability (*43*) and folding rate (*12*, *44*, *45*) of β-hairpins, and Gruebele and co-workers (*46*) have shown that the rate-limiting step during folding

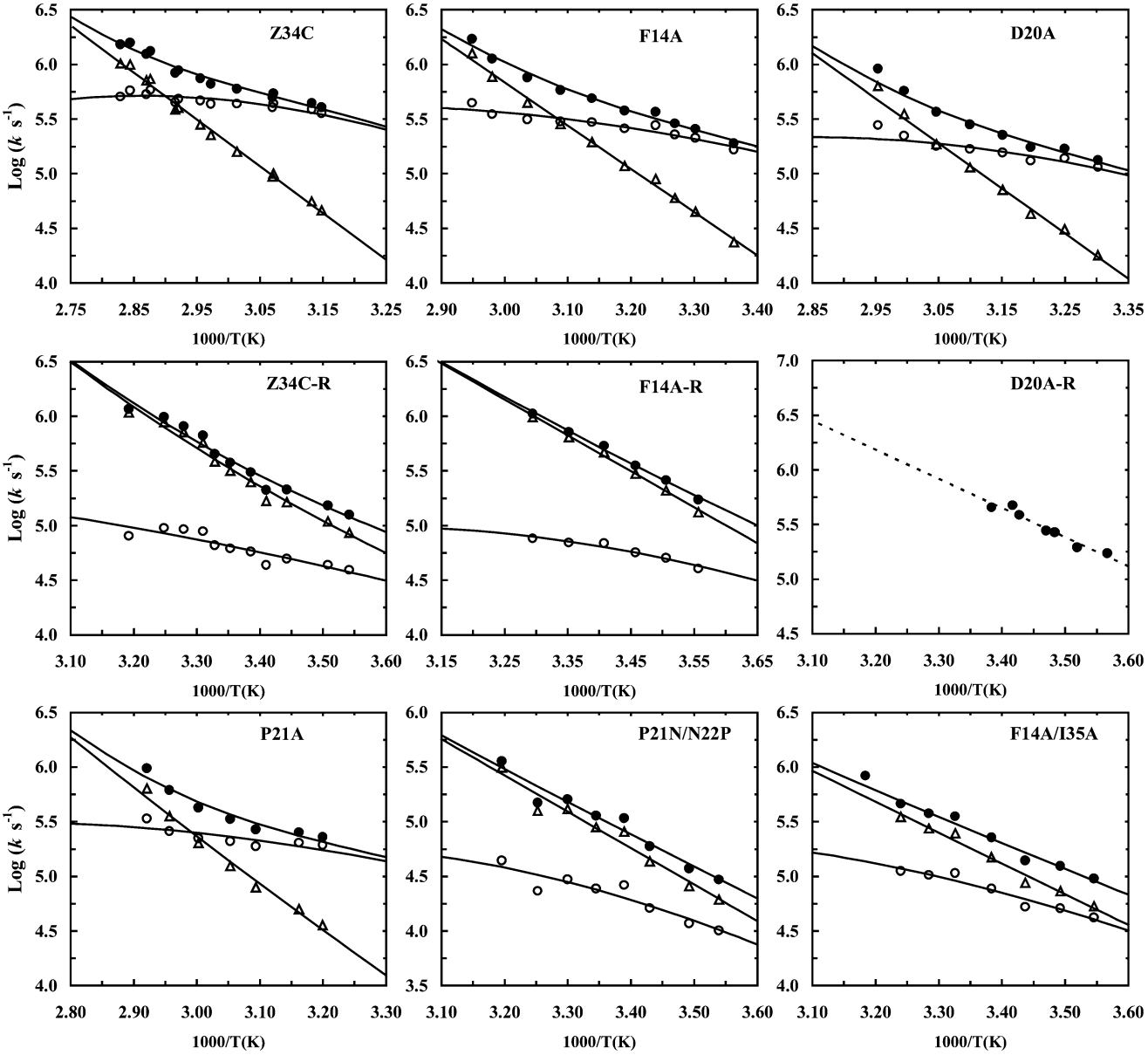

FIGURE 6: Arrhenius plot of the observed relaxation rate constant (●) as well as the folding (○) and unfolding (△) rate constants of Z34C and Z34C-R as well as their mutants, as indicated. Lines are fits to the Eyring equation; i.e., $\ln(k) = \ln(D) - \Delta G^{\ddagger}/RT$, where D was set to 1.0×10^{10} s^{-1} and $\Delta G^{\ddagger}$ is the temperature-dependent free energy of activation, which is related to other activation parameters by an equation similar to eq 3. For D20A-R, the dashed line corresponds to the linear fit to the observed relaxation rate constants.

Table 2: Folding and Unfolding Rate Constants of Z34C and Its Mutants at 50 °C[a]

	Z34C	Z34C-R	D20A	D20A-R	F14A	F14A-R	P21A	P21N/N22P	F14A/I35A
k_f^{-1} (μs)	2.5 ± 0.3	*~8.2*	5.6 ± 0.5	–	3.1 ± 0.3	*~10.4*	4.7 ± 0.6	*~20.7*	*~5.9*
k_u^{-1} (μs)	13.2 ± 0.8	*~0.3*	8.0 ± 0.4	*~0.3*	3.4 ± 0.4	*~0.2*	11.1 ± 0.7	*~1.7*	*~1.0*

[a] Italic numbers were estimated (see the text).

of the Pin WW domain, a twisted triple-stranded antiparallel β-sheet, is the formation of loop 1. The study of Fersht and co-workers (*47*) also indicated that the first loop of the YAP 65 WW domain is highly structured in the folding transition state of this β-sheet protein, but the second loop is essentially unstructured. While less studied, turns connecting antiparallel α-helices have also been shown recently to exhibit unique sequence preferences (*48*, *49*) and to be important to the stability and even the fold of helical proteins. For example, DeGrado and co-workers have demonstrated that the type and sequence of the turn in a de novo-designed helical bundle protein DF2 are critical to the α-helical hairpin conformation (*49*). Similarly, Regan and co-workers (*50*, *51*) have shown that the key linking loop sequence in the four-helix bundle protein Rop is an important determinant of the protein stability. To understand the kinetic role of the reverse turn in an α-helical hairpin, we therefore examined the folding kinetics of three mutants of Z34C in the turn region.

Mutant D20A was chosen because, according to the NMR structure of Z34C (*7*), Asp20 is part of the reverse turn and also interacts with several neighboring residues (such as Asn22 and Leu23). Therefore, replacing Asp20 with Ala, which has a much smaller turn propensity (*52*) at position *i* for a type I turn, should disrupt these interactions and result

in a decrease in the stability of the resultant α-helical hairpin conformation. As expected (Figure 3 and Table 1), the T_m of D20A is ~17 °C lower than that of Z34C. Interestingly, however, the folding rate of D20A also becomes distinctly slower (by 2.2 times) than that of the wild type, while its unfolding rate is less affected and differs from that of the parent by only 40% (Table 2). Thus, these results suggest that the consolidation of the turn imposes a free energy barrier toward the formation of the folding transition state of Z34C in which most of the native contacts involving Asp20 are formed.

The kinetic results obtained from P21A also corroborate the idea that the folding transition state of Z34C contains a nativelike turn. This is supported by the fact that the decreased stability of P21A arises almost entirely from a decrease in the folding rate (Table 2). To further demonstrate the importance of the turn sequence to the stability as well as the folding kinetics of Z34C, we also studied a double mutant, P21N/N22P. As shown (Figure 3), these mutations drastically impair the stability of the native conformation as Pro is not preferred at the $i + 2$ position for a type I turn (*52*). Since the CD thermal denaturation curve of P21N/N22P lacks a well-defined folded baseline, its folding thermodynamics could not be accurately determined. However, using the folded CD baseline of Z34C, we were able to estimate its folding thermodynamics and consequently the folding and unfolding rates of this double mutant (Figure 6). As shown (Table 2), the estimated folding rate of P21N/N22P at 50 °C is ~7.3 times slower than that of wild-type Z34C, consistent with the idea that the turn sequence is an important determinant of the folding rate of the α-helical hairpin. Nonetheless, the unfolding rate of P21N/N22P is also found to be very different from that of Z34C, suggesting that the double mutation probably causes a large change in the packing of the two helical strands, especially interactions among the hydrophobic residues, thereby leading to a decrease in the unfolding rate (see below).

Taken together, these results suggest that the free energy penalty associated with the turn formation, which is probably entropic in nature (*42*), contributes significantly to the overall folding free energy barrier of the α-helical hairpin. Consistent with this picture, Nagi and Regan (*50*) have shown that the stability of the protein Rop is correlated with the length of the glycine linker, which replaces a naturally occurring two-residue loop, where a longer length corresponds to a lower stability. Therefore, a stronger turn-promoting sequence would help to lower the free energy barrier associated with the search for the native or quasi-native turn structure and, as a result, would increase the overall folding rate (*12*, *53*). On the other hand, the unfolding rate should not be profoundly affected because the position of the transition state is not changed drastically with respect to the position of the folded state. Since the turn composition can also affect the side chain paring along the interface between two helices, it would not be surprising, therefore, if a modest change is also observed in the unfolding rate when a turn residue is changed.

The results discussed above also carry implications for understanding the kinetic role of loops, turns, cross-linkers, and any other type of structural elements that are used by proteins to connect two pieces of secondary structures (*54*). While in specific cases it may be specifically engineered and required for function, a structural linker found in proteins may assume either an active or a passive role in folding (*55*−*57*). First, it could act as a folding nucleation site, such as the reverse turn found in Z34C, so that a "preferred sequence" can increase the folding rate by efficiently lowering the folding free energy barrier. For oligomeric proteins, a linker can also provide the benefit of increasing the effective concentration of the subunits (*56*). Second, a linker could enhance the stability of the folded state by acting as a conformational constraint, such as the disulfide bond in the current case, which prevents unfolding by effectively decreasing the unfolding rate. Zhou et al. have recently discussed in detail how proteins might use such entropy-based strategies to increase the folding stability (*40*). Third, a structural linker could simply provide the connectivity needed for the polypeptide chain and have little effect on either the folding or unfolding kinetics.

Effect of the Hydrophobic Cluster on the Folding Kinetics. As suggested by the study of Wells and co-workers (*7*), the hydrophobic interactions among a group of hydrophobic amino acids, including Phe14 and Ile35, also contribute to the stabilization of the native α-helical hairpin fold of Z34C. To examine the kinetic role of this hydrophobic cluster, we further studied the folding kinetics of two mutants, F14A and F14A/I35A. As indicated by the CD measurements, the T_m of F14A is roughly 20 °C lower than that of the wild type, indicating that the hydrophobic interaction is indeed an important determinant of the α-helical hairpin stability. What is more, we found that the folding rate of F14A is similar to that of the parent. For example, at 50 °C (near the T_m of F14A) the folding time of F14A is 3.1 μs, which is comparable to that (2.5 μs) obtained for Z34C at the same temperature. In contrast, the unfolding time of F14A is significantly decreased, e.g., from 13.2 to 3.4 μs at 50 °C, compared to that of Z34C (Table 2). Consistently, F14A/I35A exhibits similar behaviors. Compared to the parent, this double mutant becomes exceedingly unstable. However, the kinetic results indicate that the decrease in its folding stability can be attributed to the increase in the unfolding rate. Taken together, therefore, these results suggest that the major kinetic role of the hydrophobic cluster is to increase the free energy barrier for unfolding, similar to that observed in β-hairpin folding (*12*). Since the unfolding process is entropically favorable, a larger unfolding free energy barrier thus arises from a stronger hydrophobic interaction. Furthermore, these results also corroborate the conclusion reached above with respect to the role of the disulfide cross-linker. While the disulfide bond provides a covalent linkage between the two helices and, thus, leads to the strongest stabilization effect, its underlying role, as discussed above, is to decrease the unfolding rate. Although not studied in this case, interchain ionic interactions may exhibit similar behaviors. For example, Matthews and co-workers (*58*) have shown that most of the intermolecular salt bridges in the coiled coil GCN4-p1 appear to play a critical role in stabilizing the native state structure but not the folding transition state.

Taken together, our results support an α-helical hairpin folding mechanism in which the transition state ensemble contains a well-structured native or quasi-native turn. Therefore, a strong turn-promoting sequence enhances the overall stability of the native fold by primarily increasing its folding rate, whereas other stabilizing interactions, such

as the hydrophobic interaction and even the disulfide cross-linker, are primarily utilized to decrease the unfolding rate. Interestingly, β-hairpin folding has been suggested to follow a similar mechanism (*12*). Given the structural resemblance between these two structural motifs, such a similarity is not at all surprising.

The results obtained here are also interesting in the context of protein structure evolution. For example, the α-helical hairpin motif is the common denominator of the so-called helix−turn−helix (HTH) domain (*59*, *60*), which consists of three helices that form a right-handed helical bundle with a partly open configuration and is ubiquitously found in various transcription factors (*2*). Among these three helices, the second and third helices constitute a helix−turn−helix motif and have been shown to be a critical determinant of their interaction with DNA (*59*−*61*), whereas the remaining helix has been suggested to stabilize the folded structure (*62*), akin to the role of the disulfide cross-linker in Z34C. Also consistent with our results, it was found that the characteristic turn, which defines the helix−turn−helix structure, typically does not tolerate insertions or distortions. However, the loop linking helix 1 and helix 2 shows far greater variability and may accommodate several modifications in the different classes of HTH domains (*2*). Thus, this loop may only provide the needed connectivity between helices and has little effect on the folding kinetics of the native structure. Therefore, it would be interesting to study the folding kinetics of a series of structurally related proteins, beginning with the simplest structure, and to examine how the folding rate and mechanism evolve as a function of the complexity of the folded structure. This may prove to be an effective bottom-up approach that can help in dissecting the many delicate yet correlated factors that control how large proteins fold.

CONCLUSION

In summary, we have studied the thermal stability and folding kinetics of an α-helical hairpin (Z34C) using static CD and IR and time-resolved IR spectroscopies. Our results provided new insights into the understanding of the kinetics of α-helical hairpin folding and revealed the kinetic role of several key structural elements. In particular, our results suggested a folding model in which the rate-limiting step corresponds to the consolidation of the turn. Thus, a good turn-promoting sequence and a strong interstrand hydrophobic cluster can help to stabilize the folded conformation of α-helical hairpins. Nevertheless, the former increases the stability of an α-helical hairpin primarily by increasing its folding rate, whereas the latter does that primarily by decreasing its unfolding rate. In addition, we found that the kinetic role of the disulfide cross-linker in Z34C is to primarily prevent the native state from unfolding, similar to that of the hydrophobic cluster.

REFERENCES

1. Huffman, J. L., and Brennan, R. G. (2002) Prokaryotic transcription regulators: More than just the helix-turn-helix motif, *Curr. Opin. Struct. Biol. 12*, 98−106.
2. Aravind, L., Anantharaman, V., Balaji, S., Babu, M. M., and Iyer, L. M. (2005) The many faces of the helix-turn-helix domain: Transcription regulation and beyond, *FEMS Microbiol. Rev. 29*, 231−262.
3. Fezoui, Y., Weaver, D. L., and Osterhout, J. J. (1994) De novo design and structural characterization of an α-helical hairpin peptide: A model system for the study of protein folding intermediates, *Proc. Natl. Acad. Sci. U.S.A. 91*, 3675−3679.
4. Karplus, M., and Weaver, D. L. (1994) Protein folding dynamics: The diffusion-collision model and experimental data, *Protein Sci. 3*, 650−668.
5. Hoffmann, D., and Knapp, E.-W. (1997) Folding pathways of a helix-turn-helix model protein, *J. Phys. Chem. B 101*, 6734−6740.
6. Fersht, A. R., and Daggett, V. (2002) Protein folding and unfolding at atomic resolution, *Cell 108*, 573−582.
7. Starovasnik, M. A., Braisted, A. C., and Wells, J. A. (1997) Structural mimicry of a native protein by a minimized binding domain, *Proc. Natl. Acad. Sci. U.S.A. 94*, 10080−10085.
8. Braisted, A. C., and Wells, J. A. (1996) Minimizing a binding domain from protein A, *Proc. Natl. Acad. Sci. U.S.A. 93*, 5688−5692.
9. Imperiali, B., and Ottesen, J. J. (1999) Uniquely folded miniprotein motifs, *J. Pept. Res. 54*, 177−184.
10. DeGrado, W. F., Summa, C. M., Pavone, V., Nastri, F., and Lombardi, A. (1999) De novo design and structural characterization of proteins and metalloproteins, *Annu. Rev. Biochem. 68*, 779−819.
11. Muñoz, V., Thompson, P. A., Hofrichter, J., and Eaton, W. A. (1997) Folding dynamics and mechanism of β-hairpin formation, *Nature 390*, 196−199.
12. Du, D., Zhu, Y., Huang, C.-Y., and Gai, F. (2004) Understanding the key factors that control the rate of β-hairpin folding, *Proc. Natl. Acad. Sci. U.S.A. 101*, 15915−15920.
13. Huang, C.-Y., Klemke, J. W., Getahun, Z., DeGrado, W. F., and Gai, F. (2001) Temperature-dependent helix-coil transition of an alanine based peptide, *J. Am. Chem. Soc. 123*, 9235−9238.
14. Huang, C.-Y., Getahun, Z., Zhu, Y., Klemke, J. W., DeGrado, W. F., and Gai, F. (2002) Helix formation via conformation diffusion search, *Proc. Natl. Acad. Sci. U.S.A. 99*, 2788−2793.
15. Matouschek, A., Kellis, J. T., Jr., Serrano, L., and Fersht, A. R. (1989) Mapping the transition state and pathway of protein folding by protein engineering, *Nature 340*, 122−126.
16. Dyer, R. B., Gai, F., Woodruff, W. H., Gilmanshin, R., and Callender, R. H. (1998) Infrared studies of fast events in protein folding, *Acc. Chem. Res. 31*, 709−716.
17. Krimm, S., and Bandekar, J. (1986) Vibrational spectroscopy conformation of peptides, polypeptides, and proteins, *Adv. Protein Chem. 38*, 181−364.
18. Gilmanshin, R., Williams, S., Callender, R. H., Woodruff, W. H., and Dyer, R. B. (1997) Fast events in protein folding: Relaxation dynamics and structure of the I form of apomyoglobin, *Biochemistry 36*, 15006−15012.
19. Callender, R. H., Dyer, R. B., Gilmanshin, R., and Woodruff, W. H. (1998) Fast events in protein folding: The time evolution of primary processes, *Annu. Rev. Phys. Chem. 49*, 173−202.
20. Zhu, Y., Alonso, D. O. V., Maki, K., Huang, C.-Y., Lahr, S. J., Daggett, V., Roder, H., DeGrado, W. F., and Gai, F. (2003) Ultrafast folding of α3D: A de novo designed three-helix bundle protein, *Proc. Natl. Acad. Sci. U.S.A. 100*, 15486−15491.
21. Walsh, S. T. R., Cheng, R. P., Wright, W. W., Alonso, D. O. V., Daggett, V., Vanderkooi, J. M., and DeGrado, W. F. (2003) The hydration of amides in helices: A comprehensive picture from molecular dynamics, IR, and NMR, *Protein Sci. 12*, 520−531.
22. Xu, Y., Oyola, R., and Gai, F. (2003) Infrared study of the stability and folding kinetics of a 15-residue β-hairpin, *J. Am. Chem. Soc. 125*, 15388−15394.
23. Searle, M. S., and Ciani, B. (2004) Design of β-sheet systems for understanding the thermodynamics and kinetics of protein folding, *Curr. Opin. Struct. Biol. 14*, 458−464.
24. Serrano, L. (2000) The relationship between sequence and structure in elementary folding units, *Adv. Protein Chem. 53*, 49−85.
25. McCallister, E. L., Alm, E., and Baker, D. (2000) Critical role of β-hairpin formation in protein G folding, *Nat. Struct. Biol. 7*, 669−673.
26. Walkenhorst, W. F., Edwards, J. A., Markley, J. L., and Roder, H. (2002) Early formation of a β hairpin during folding of staphylococcal nuclease H124L as detected by pulsed hydrogen exchange, *Protein Sci. 11*, 82−91.
27. Schönbrunner, N., Pappenberger, G., Scharf, M., Engels, J., and Kiefhaber, T. (1997) Effect of preformed correct tertiary interactions on rapid two-state tendamistat folding: Evidence for hairpins as initiation sites for β-sheet formation, *Biochemistry 36*, 9057−9065.

28. Roder, H., Maki, K., and Cheng, H. (2006) Early events in protein folding explored by rapid mixing methods, *Chem. Rev. 106*, 1836−1861.
29. Betz, S. F. (1993) Disulfide bonds and the stability of globular proteins, *Protein Sci. 2*, 1551−1558.
30. Petersen, M. T., Jonson, P. H., and Petersen, S. B. (1999) Amino acid neighbors and detailed conformational analysis of cysteines in proteins, *Protein Eng. 12*, 535−548.
31. Kuroda, Y., Nakai, T., and Ohkubo, T. (1994) Solution structure of a de novo helical protein by 2D-NMR spectroscopy, *J. Mol. Biol. 236*, 862−868.
32. Moran, L. B., Schneider, J. P., Kentsis, A., Reddy, G. A., and Sosnick, T. R. (1999) Transition state heterogeneity in GCN4 coiled coil folding studied by using multisite mutations and crosslinking, *Proc. Natl. Acad. Sci. U.S.A. 96*, 10699−10704.
33. Shimaoka, M., Lu, C., Salas, A., Xiao, T., Takagi, J., and Springer, T. A. (2002) Stabilizing the integrin α M inserted domain in alternative conformations with a range of engineered disulfide bonds, *Proc. Natl. Acad. Sci. U.S.A. 99*, 16737−16741.
34. Johnson, C. M., Oliveberg, M., Clarke, J., and Fersht, A. R. (1997) Thermodynamics of denaturation of mutants of barnase with disulfide crosslinks, *J. Mol. Biol. 268*, 198−208.
35. Vogl, T., Brengelmann, R., Hinz, H.-J., Scharf, M., Loetzbeyer, M., and Engels, J. W. (1995) Mechanism of protein stabilization by disulfide bridges: Calorimetric unfolding studies on disulfide-deficient mutants of the α-amylase inhibitor tendamistat, *J. Mol. Biol. 254*, 481−496.
36. Welker, E., Wedemeyer, W. J., Narayan, M., and Scheraga, H. A. (2001) Coupling of conformational folding and disulfide-bond reactions in oxidative folding of proteins, *Biochemistry 40*, 9059−9064.
37. Abkevich, V. I., and Shakhnovich, E. I. (2000) What can disulfide bonds tell us about protein energetics, function and folding: Simulations and bioinformatics analysis, *J. Mol. Biol. 300*, 975−985.
38. Mason, J. M., Gibbs, N., Sessions, R. B., and Clarke, A. R. (2002) The influence of intramolecular bridges on the dynamics of a protein folding reaction, *Biochemistry 41*, 12093−12099.
39. Kubelka, J., Hofrichter, J., and Eaton, W. A. (2004) The protein folding 'speed limit', *Curr. Opin. Struct. Biol. 14*, 76−88.
40. Zhou, H. X. (2004) Loops, linkages, rings, catenanes, cages, and crowders: Entropy-based strategies for stabilizing proteins, *Acc. Chem. Res. 37*, 123−130.
41. Camarero, J. A., Fushman, D., Sato, S., Giriat, I., Cowburn, D., Raleigh, D. P., and Muir, T. W. (2001) Rescuing a destabilized protein fold through backbone cyclization, *J. Mol. Biol. 308*, 1045−1062.
42. Zhou, H. X. (2005) How do biomolecular systems speed up and regulate rates? *Phys. Biol. 2*, R1−R25.
43. Gellman, S. H. (1998) Minimal model systems for β-sheet secondary structure in proteins, *Curr. Opin. Chem. Biol. 2*, 717−725.
44. Dyer, R. B., Maness, S. J., Peterson, E. S., Franzen, S., Fesinmeyer, R. M., and Andersen, N. H. (2004) The mechanism of β-hairpin formation, *Biochemistry 43*, 11560−11566.
45. Chen, R. P. Y., Huang, J. J. T., Chen, H.-L., Jan, H., Velusamy, M., Lee, C.-T., Fann, W., Larsen, R. W., and Chan, S. I. (2004) Measuring the refolding of β-sheets with different turn sequences on a nanosecond time scale, *Proc. Natl. Acad. Sci. U.S.A. 101*, 7305−7310.
46. Jäger, M., Nguyen, H., Crane, J. C., Kelly, J. W., and Gruebele, M. (2001) The folding mechanism of a β-sheet, *J. Mol. Biol. 311*, 373−393.
47. Ferguson, N., Pires, J. R., Toepert, F., Johnson, C. M., Pan, Y. P., Volkmer-Engert, R., Schneider-Mergener, J., Daggett, V., Oschkinat, H., and Fersht, A. (2001) Using flexible loop mimetics to extend Φ-value analysis to secondary structure interactions, *Proc. Natl. Acad. Sci. U.S.A. 98*, 13008−13013.
48. Efimov, A. V. (1991) Structure of α-α hairpins with short connections, *Protein Eng. 4*, 245−250.
49. Lahr, S. J., Engel, D. E., Stayrook, S. E., Maglio, O., North, B., Geremia, S., Lombardi, A., and DeGrado, W. F. (2005) Analysis and design of turns in α-helical hairpins, *J. Mol. Biol. 346*, 1441−1454.
50. Nagi, A. D., and Regan, L. (1997) An inverse correlation between loop length and stability in a four-helix-bundle protein, *Folding Des. 2*, 67−75.
51. Predki, P. F., Agrawal, V., Brunger, A. T., and Regan, L. (1996) Amino-acid substitutions in a surface turn modulate protein stability, *Nat. Struct. Biol. 3*, 54−58.
52. Hutchinson, E. G., and Thornton, J. M. (1994) A revised set of potentials for β-turn formation in proteins, *Protein Sci. 3*, 2207−2216.
53. Kobayashi, N., Honda, S., Yoshii, H., and Munekata, E. (2000) Role of side-chains in the cooperative β-hairpin folding of the short C-terminal fragment derived from streptococcal protein G, *Biochemistry 39*, 6564−6571.
54. Brunet, A. P., Huang, E. S., Huffine, M. E., Loeb, J. E., Weltman, R. J., and Hecht, M. H. (1993) The role of turns in the structure of an α-helical protein, *Nature 364*, 355−358.
55. Liang, H., Sandberg, W. S., and Terwilliger, T. C. (1993) Genetic fusion of subunits of a dimeric protein substantially enhances its stability and rate of folding, *Proc. Natl. Acad. Sci. U.S.A. 90*, 7010−7014.
56. Robinson, C. R., and Sauer, R. T. (1996) Equilibrium stability and sub-millisecond refolding of a designed single-chain Arc repressor, *Biochemistry 35*, 13878−13884.
57. Zhou, H. X. (2001) Single-chain versus dimeric protein folding: Thermodynamic and kinetic consequences of covalent linkage, *J. Am. Chem. Soc. 123*, 6730−6731.
58. Ibarra-Molero, B., Zitzewitz, J. A., and Matthews, C. R. (2004) Salt-bridges can stabilize but do not accelerate the folding of the homodimeric coiled-coil peptide GCN4-p1, *J. Mol. Biol. 336*, 989−996.
59. Ohlendorf, D. H., Anderson, W. F., and Matthews, B. W. (1983) Many gene-regulatory proteins appear to have a similar α-helical fold that binds DNA and evolved from a common precursor, *J. Mol. Evol. 19*, 109−114.
60. Sauer, R. T., Yocum, R. R., Doolittle, R. F., Lewis, M., and Pabo, C. O. (1982) Homology among DNA-binding proteins suggests use of a conserved super-secondary structure, *Nature 298*, 447−451.
61. Ohlendorf, D. H., Anderson, W. F., Fisher, R. G., Takeda, Y., and Matthews, B. W. (1982) The molecular basis of DNA-protein recognition inferred from the structure of cro repressor, *Nature 298*, 718−723.
62. Ebneth, A., Schweers, O., Thole, H., Fagin, U., Urbanke, C., Maass, G., and Wolfes, H. (1994) Biophysical characterization of the c-myb DNA-binding domain, *Biochemistry 33*, 14586−14593.

BI0615745